CrossMark

One-pot synthesis of urchin-like ZnO nanostructure and its enhanced acetone gas sensing properties

Weiwei Guo[1]

Abstract A hierarchical urchin-like ZnO nanostructure was successfully synthesized via a facile and efficient hydrothermal method. The sample was characterized by XRD, FESEM, TEM, BET, UV–Vis DRS and Photoluminescence (PL) techniques. The urchin-like ZnO is assembled by many nanorods and has the average size of 1.5 μm. The BET surface and pore volume of urchin-like ZnO were measured to be 53.9 m^2 g^{-1} and 0.073 cm^3 g^{-1}. The hydrothermal time and pH value have important effect on the morphology. UV–Vis spectra show that a narrower band gap for the urchin-like ZnO as compared to commercial ZnO. PL spectra indicate that the urchin like ZnO has the higher donors and fewer acceptors than that of commercial ZnO. Furthermore, the urchin-like ZnO nanostructure exhibited excellent gas sensing properties towards acetone, indicating that the as-prepared urchin-like ZnO is a promising material for gas sensors.

1 Introduction

With the rapid development of industrialization and urbanization in the past few decades, environment pollution caused by the volatilization of hazardous gases has become an important issue. Acetone, as a widely used solvent in industry and laboratory, can volatilize easily and affect human health when its concentration is higher than 173 ppm [1–3]. Although the study on acetone sensor is necessary, the present reported acetone sensors have suffered from some disadvantages, such as poor selectivity, inadequate sensitivity [4–6]. Therefore, it is highly desirable to develop high performance sensors for rapidly selective detection of acetone.

Among various metal oxide semiconductor (MOS)-based gas sensing materials studied so far, ZnO, as a non-toxicity, high transparency, wide direct band gap (3.37 eV), large exciton binding energy (0.060 eV), excellent thermal and chemical stability compound semiconductor, has been proved to be one of the promising materials for gas sensors [7–11]. It's well known that the properties of ZnO depend highly on its nanostructures, including crystal size, orientation and morphology. Recently, the self-assembly from the nanoscaled building block to the complex hierarchical structures [12], has been a hot topic in the research. Hierarchical structures may provide more spaces for gases to diffuse into the inner of the sensing film [13, 14]. For example, Alenezi et al. [15] prepared the hierarchical structures based on ZnO nanowire or nanodisk which possessed high surface area to volume ratios and an increased proportion of exposed active planes. Those hierarchical ZnO structures displayed significantly improved sensitivity and fast response to acetone in comparison to other mono-morphological ZnO. Ko et al. synthesized nano-tree like ZnO hierarchical nanostructures which greatly enhanced the surface area [16, 17]. However, most of hierarchical ZnO architectures were fabricated successfully with the assistance of surfactants or templates. It is well known that the addition of ionic liquid, complexing agent or template usually introduces the impurities. Furthermore, these syntheses also have a high cost and involve complicated multi steps [18, 19]. Therefore, it is very significant to develop a facile,

✉ Weiwei Guo
  shendaguowei@163.com

[1] Chongqing Key Laboratory of Catalysis and Functional Organic Molecules, College of Environment and Resources, Chongqing Technology and Business University, Chongqing 400067, People's Republic of China

shape and size-controlled self- assembly route for the formation of ZnO complex architectures assembled from1D nanocrystals.

In this paper, urchin-like ZnO was successfully prepared by a simple hydrothermal method in the absence of surfactant and template. The structure, BET surface, band gap, surface defects and gas sensing properties of the as-prepared sample are investigated. In addition, the possible gas sensing mechanism of urchin-like ZnO nanostructure is discussed.

2 Experimental

2.1 Synthesis

All chemical reagents were of analytical grade (Chuandong Chemical Reagent Co., Ltd.) and used as-received with no further purification. The urchin-like ZnO were prepared by a simple one pot hydrothermal method. In a typical synthesis process, 0.2 g Zinc powders was added into 40 mL NaOH aqueous solution with the pH value of 13.5 and magnetically stirred for 1 h, the solution was moved to a 50 mL Teflon-lined stainless steel autoclave, sealed, and maintained at 140 °C for 8 h. After the hydrothermal procedure, the autoclave cooled naturally down to room temperature. Finally, the white products on the bottom of the autoclave were harvested upon pursuing centrifugation, washing away unexpected ions with distilled water and absolute ethanol several times to remove possible impurities. The precipitates were dried in ambient air at 60 °C for 10 h to get ZnO powders.

2.2 Characterization

Microstructure analysis was conducted by the X-ray diffraction (XRD), scanning electron microscopy (SEM), and transmission electron microscopy (TEM). For the XRD, a Rigaku D/Max-1200X diffractometry with $Cu\ K_a$ radiation operated at 40 kV and 200 mA was applied. Surface morphologies of the samples were observed using a Hitachi S-4300 SEM. Microstructures and chemical composition were analyzed using the JEOL JEM-2010F electron microscope operated at an accelerating voltage of 200 kV. Specific surface area was measured upon the multipoint Brunauer–Emmett–Teller (BET) analysis of nitrogen adsorption isotherms, which were recorded on a surface area analyzer (Micromeritics, ASAP 2020 M). The UV–Vis diffuse reflection spectra (UV–Vis DRS) were obtained for the dry-pressed disk samples using a scan UV–Vis spectrophotometer (UV-2450, Shimadzu, Japan). Photoluminescence (PL, F-7000, HITACHI, Japan) was used to investigate the optical properties of the obtained samples.

2.3 Sensor fabrication and measurement

Gas sensors were fabricated by firstly mixed the products with distilled water to form homogeneous suspensions and then pasted on commercial ceramic substrates with Ag-Pd interdigitated electrodes (Fig. 1). The thickness of the pasted films spans the range from 1 to 2 mm and dried at 55 °C in air to form a solid pasted films for 2 h. Further, the gas sensor was put on a heating plate in the test chamber by pressing firmly with two probes (Fig. 1). Two adjustable probes were pressed on the sensor electrodes to collect electrical signals. The gas sensing behaviors of the sensors were tested on the heating ceramic plate of the CGS-1TP instrument. The sensor was preheated for about 30 min at certain target temperature until the resistance of the materials reached a stable range, and then was sealed in an 18 L test chamber. Here, the sensitivity of the sensor is defined as S = Ra/Rg, where Ra and Rg are the resistances of sensor in air and target gas, respectively.

3 Results and discussion

3.1 Structural and morphological characteristics

Figure 2 shows the X-ray powder diffraction (XRD) pattern of the products. All the diffraction peaks in XRD are fully matched with pure wurtzite phase of ZnO crystals (JCPDS: 36-1451). No other peaks have been detected in XRD patterns, confirming that the synthesized products exhibit pure ZnO crystal with hexagonal wurtzite phase.

The morphology of the samples was investigated by field emission scanning electron microscopy (FESEM). Figure 3 shows typical FESEM images of the ZnO sample at different magnification. The low magnification FESEM image (Fig. 3a) clearly displayed that the products are composed of uniform urchin-like structures. No other morphologies can be found in Fig. 3a, which indicated the high uniformity of the as-obtained products. The detailed morphology information about urchin-like ZnO is presented in an enlarged-magnification FESEM (Fig. 3b, c), indicating that the size of urchin-like ZnO was about 1.5 μm and assembled by many nanorods. Higher magnification FESEM image is shown in Fig. 3d. As seen from it, the diameter of the ZnO nanorods was about 20 nm. On the basis of the above results, the as-prepared urchin-like structure can be generally classified as hierarchical structures.

Further detailed structural analysis of urchin-like ZnO was carried out using TEM. Figure 4a shows the TEM image of representative urchin-like ZnO nanostructures. It can be seen that the size and shape of product were similar to those of the FESEM observations. A high-magnification
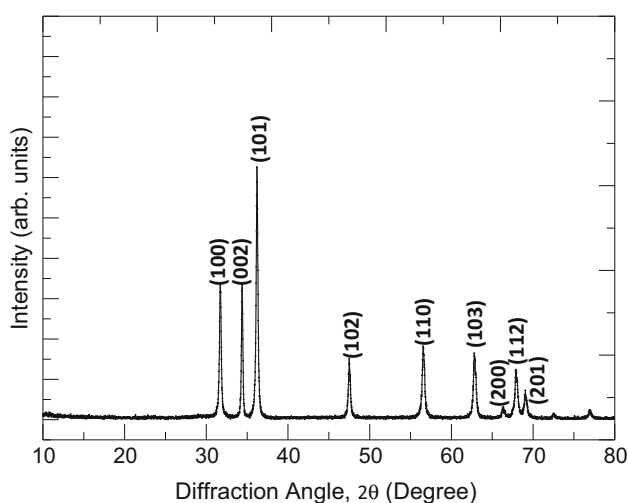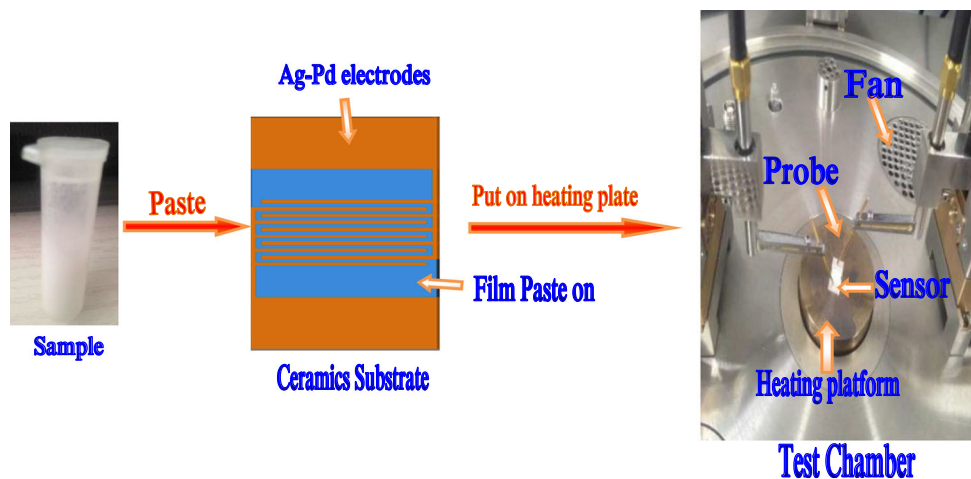
TEM (Fig. 4b) image presents that the diameter of nanorod was about 20 nm. The high-resolution transmission electron microscopy (HRTEM) image (Fig. 4c) showed fringe distance of 0.2636 nm corresponding to the distance between two adjacent (0002) planes of ZnO, suggesting that the (0001) direction (c-axis) was the preferential growth direction of ZnO nanorod. The selected-area electron diffraction (SAED) pattern of an individual ZnO nanorod (Fig. 4d) confirms that the as-synthesized products were single crystalline in structure.

3.2 Effect of time and pH value on the morphology

To reveal the formation process of this unique urchin like structure, morphology evolution of the urchin-like ZnO is investigated in detail as a function of reaction time, as shown in Fig. 5. From Fig. 5a, the Zn powders are irregular in shape and have a large size of 3–5 μm. Once the powders are added into the sodium hydroxide solution for 1 h,

surface of the powders turns coarse and loose (Fig. 5b). After the alkaline treatment for 3 h, size of the powders becomes smaller and some irregular powders are evolved gradually to a spherical structure with an average size of 2–3 μm (Fig. 5c). As the reaction time is increased to 3 h, the urchin-like ZnO are formed. Further extension of the hydrothermal time to 12 h would destroy the urchin like structure (Fig. 5d) and the sarciniform ZnO formed, implying that an appropriate time is needed to produce the urchin-like ZnO.

pH value was also essential to the morphologies of the ZnO structures. When the pH value of the solution is 13, the irregular stone like morphologies were formed (Fig. 6a), which is due to the inadequate supply of OH^- and inefficient etching for the Zn powders. As the pH of the solution was increased to 14, dispersive rod-like ZnO formed (Fig. 6b), which was due to the excessive supply of OH^- to dissolve the Zn powders quickly. These process produced a lot of growth units of $Zn(OH)_2$, and grow along the (0001) direction to form the rod-like ZnO.

3.3 BET measurement

The nitrogen adsorption–desorption isotherms and corresponding pore size distribution curves of the ZnO sample are displayed in Fig. 7. According to the Brunauer-Deming-Deming-Teller (BDDT) classification, the majority of the physisorption isotherms are close to type IV, which reflects the presence of mesopores in ZnO sample. This result is also demonstrated by the pore-size distribution curves. Moreover, the shape of the hysteresis loops is of type H3, suggesting the existence of slitlike pores [20]. This result is in agreement with the SEM observation. The inset of Fig. 7 depicts the corresponding pore size distribution curves of the samples. The pore-size distribution range for the samples is broad, in the range of 5–90 nm, and unimodal with some small mesopores (20.1 nm),

Fig. 3 **a** Low magnification
SEM images of the as-prepared
ZnO, **b** and **c** enlarged SEM
images of single urchin-like
ZnO and **d** the partial enlarged
SEM image of urchin-like ZnO
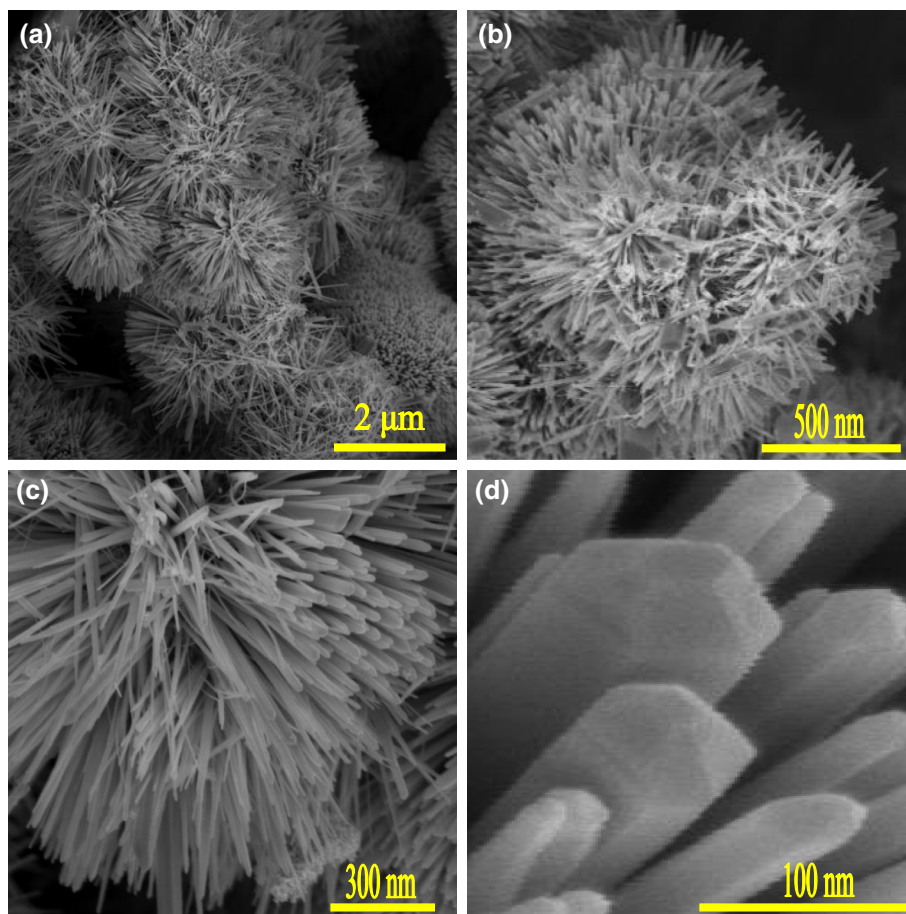
confirming the formation of mesopores [21]. The mesopores can be attributed to the pores formed among the aggregated nanorods. The BET surface area and the pore volume of urchin- like ZnO were measured to be 53.9 m^2 g^{-1} and 0.073 cm^3 g^{-1}.

3.4 Gas sensing properties

To demonstrate the potential applications, gas sensor had been fabricated and investigated for acetone detection. For comparison, gas sensing properties of commercial ZnO powder (AR grade) were also tested. Due to the great influence of working temperature on gas-sensing performances, such as gas response, response-recovery time and selectivity, the response characteristics of sensors based on urchin-like and commercial ZnO toward acetone have been firstly investigated as a function of the operating temperature. As shown in Fig. 8a, it can be seen that the corresponding response curves of two sensors exhibit the similar trends and sensor based on urchin-like ZnO shows an obvious high response at the same operating temperature. For urchin-like ZnO, the response is increased with the increase of the operating temperature in the range of 150–450 °C, reached the highest responses at 300 °C, and

then decreased with further increasing the operating temperature. The maximum response values of urchin-like and commercial ZnO are 58.1 and 23.8, respectively. The improved response of urchin-like ZnO during the whole temperature range, compared with that of commercial ZnO sample. Obviously, the optimal working temperature of these ZnO samples is selected at 300 °C, which will be applied in all the gas-sensing investigations hereinafter.

Besides response value of sensing materials is an important index to evaluate their gas-sensing performances, the response and recovery characteristic is another important prerequisite for practice applications of gas sensors. As shown in Fig. 8b, the response-recovery times of sensors based on these two ZnO nanostructures have also been investigated for 10 ppm acetone within a single cycle period. It is obvious that the response and recovery process of urchin like ZnO have shorter time to maintain certain stable response compared with that of commercial ZnO. The response and recovery time of urchin like ZnO are about 42 and 10 s, respectively, while, that of commercial ZnO are 93 and 15 s.

Then, the successive response behaviors of urchin like ZnO upon being orderly exposed to the increased concentration of acetone have also been investigated and the

Fig. 4 a TEM image of urchin-like ZnO, **b** the partial HETEM image of urchin-like ZnO, **c** the HRTEM image of a single nanorod and d the corresponding SAED patterns
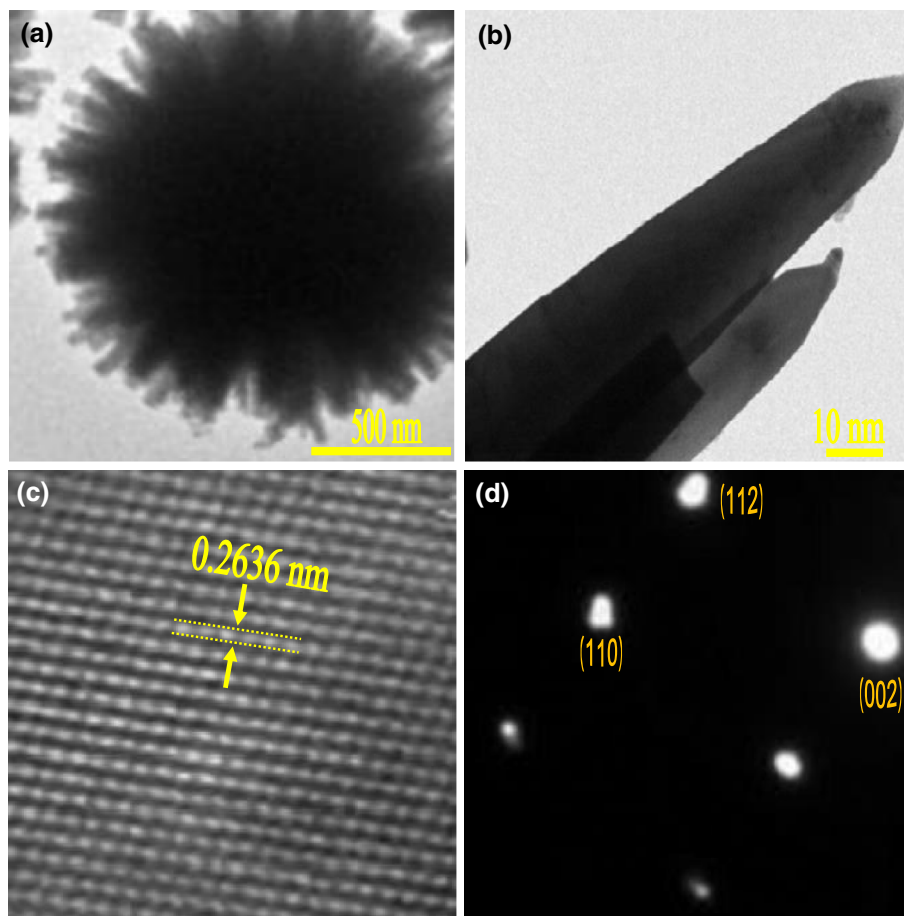
results are shown in Fig. 8c. In the whole process, the response values increased with the increase of the concentration of acetone, and the response-recovery time almost remain no change, indicating that the sensor shows good repeatability for acetone detection. The key selectivity of urchin-like ZnO has also been investigated to various testing gases with the same concentration of 10 ppm and the result is shown in Fig. 8d. Obviously, sensor based on urchin-like ZnO exhibits an obvious highest response of 58.1 to acetone and lesser effects for other testing gases, which is not higher than 20. The response value of our urchin-like ZnO to acetone is above 2.0 times higher than those of the typical interfering gas achieved at the same temperature, respectively. Among these gas traces, the sensor based on urchin-like ZnO has a satisfying capability to detect acetone in a selective manner with a high response.

3.5 UV–Vis diffuse and PL spectra analysis

The UV–Vis diffuse reflectance spectra of the as-prepared and commercial ZnO samples are shown in Fig. 9. All samples display fundamental absorption edges rising around 390 nm, which can be assigned to the intrinsic band gap absorption of ZnO [22]. It is also clearly observed that a significant red-shift in the absorption edge for the urchin-like ZnO occurs as compared to commercial ZnO (Fig. 9a). Figure 9b depicts the optical band gap (Eg) estimated from a Tauc plot of $(\alpha h\upsilon)^2$ versus photon energy (hυ) according to the K-M model [23]. The estimated Eg for the as-prepared urchin-like and commercial ZnO are 3.08 and 3.17 eV, respectively. It is apparent that urchin-like ZnO has narrower band gap compared with commercial ZnO.

To the ZnO sensor, the key influence on the sensing property may be the electric state of ZnO. It is well-known that the nonstoichiometry or crystal defect determines the electronic properties of semiconductors. The intrinsic defects of ZnO are categorized as zinc interstitial (Zn_i), zinc vacancy (V_{Zn}), oxygen interstitial (O_i), oxygen vacancy (V_O), oxygen antisite (O_{Zn}) and Zn antisite (Zn_O) [24]. Of the six defects, Zn_O are unlikely to be stable under equilibrium conditions due to their high formation energies; Zni and VO give rise to free electrons (i.e., donor) in ZnO crystal, while V_{Zn}, O_i, and O_{Zn} consume free electrons (i.e., acceptor) [25]. In equilibrium, the amount of released free electrons is higher than that of trapped electrons making ZnO to be an n-type semiconductor. The relative content of donors and acceptors determines the

Fig. 5 SEM images of the Zn powders for different hydrothermal time: **a** Zn powders, **b** 1 h, **c** 3 h and **d** 12 h
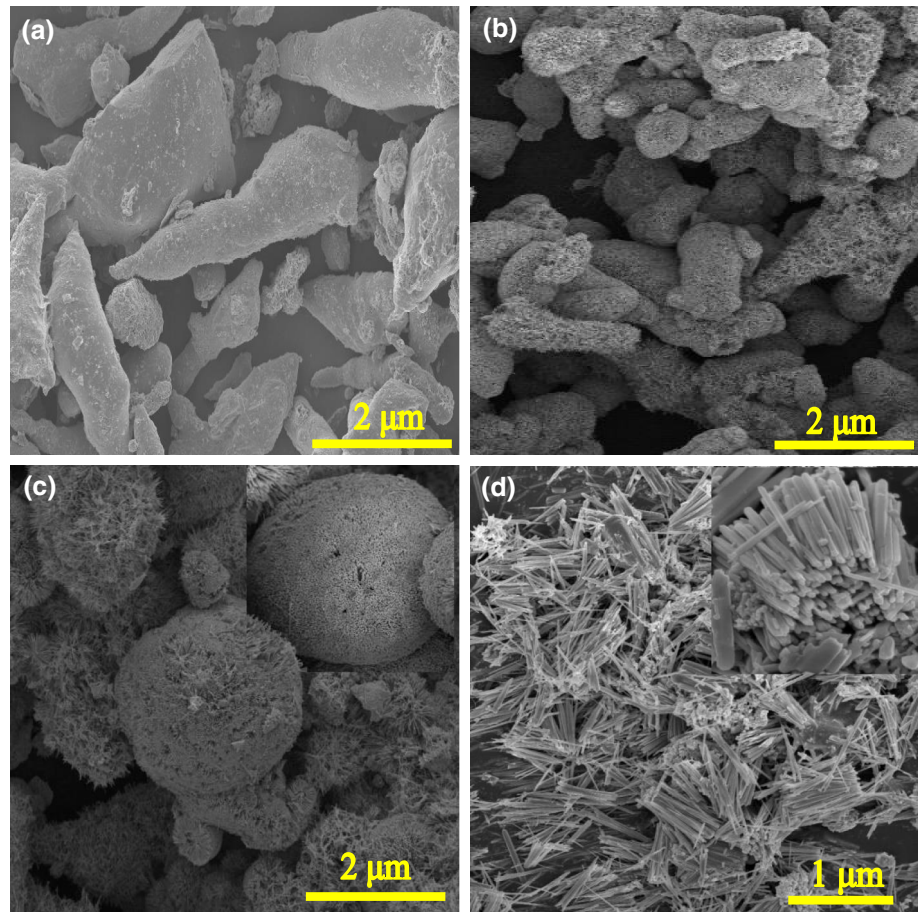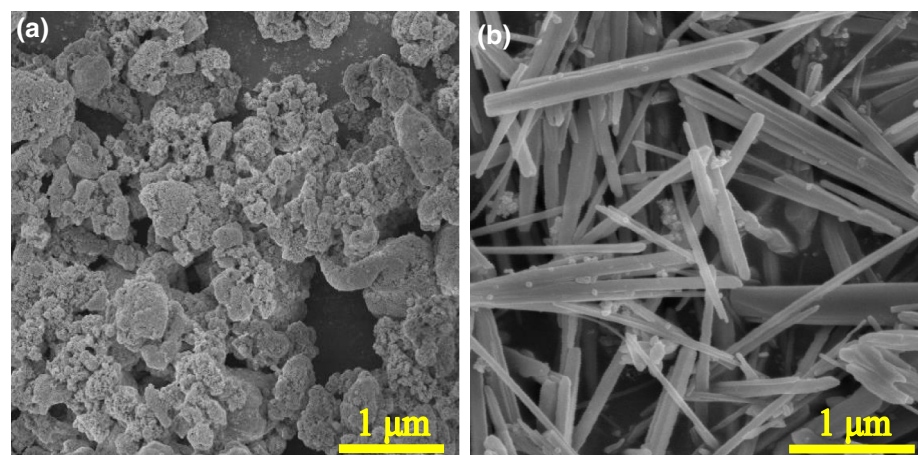

Fig. 6 SEM images of the Zn powders in the solution with different pH value: **a** pH = 13 and **b** pH = 14

semiconductive property of ZnO. The PL spectrum of ZnO originates from either the photo induced electron_hole recombination or the intrinsic defects [26]. Therefore, we used the PL spectroscopy methods to study the defect structures of urchin like and commercial ZnO. As shown in Fig. 10, according to their originations, the whole PL spectrum in the range 360–600 nm can be Gaussian deconvoluted into seven parts. The sharp ultraviolet (UV)

peak at 376 nm is attributed to the exciton emission from conduction band to valence band (CB–VB combination). The UV emission peaks at 395 and 420 nm can be indexed to the shallow donor Zn_i. The peak at 460 nm is associated with V_{Zn}. The peak at 490 nm is attributed to V_O. The peak at 520 nm is related to O_{Zn}, while the origins of yellow and orange luminescence above 540 nm are attributed to O_i [27]. Summarily, the percentages of donors ($Zn_i + V_O$)
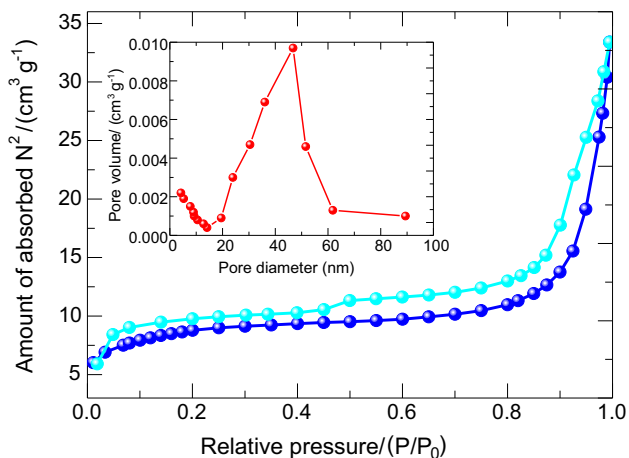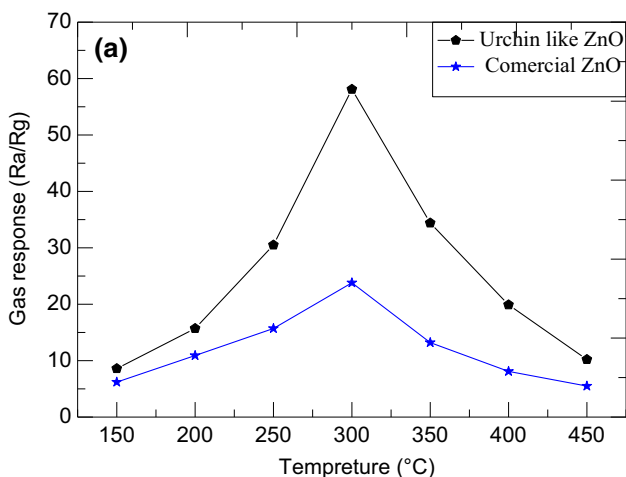
Fig. 7 N$_2$ adsorption–desorption isotherm and the corresponding pore size distribution of the urchin like ZnO samples

and acceptors ($V_{Zn} + O_i + O_{Zn}$) can be obtained by peak separation from Fig. 10, and it is found that urchin like ZnO has the higher donors (70.9 %) and fewer acceptors (27.1 %) than that of commercial ZnO sample [donors (58.46 %), acceptors (41.5 %)].

3.6 Gas sensing mechanism

It's well known that, as a typical n-type metal oxide semiconductor sensor, the gas sensing mechanism of ZnO-based sensor belongs to the surface-controlled type and is based on the conductivity changes caused by the adsorption and desorption of the gas molecules on the materials surface [28, 29].

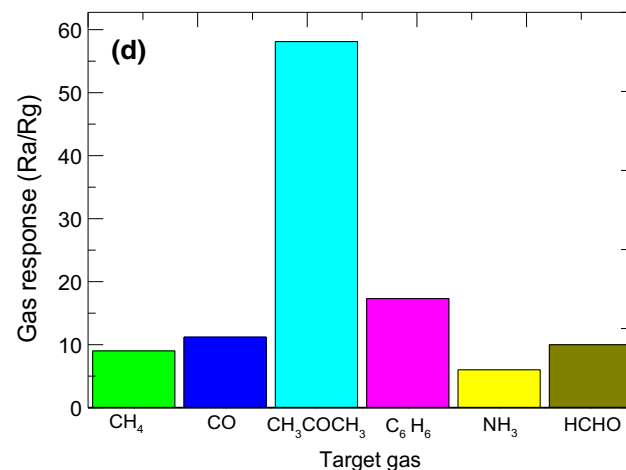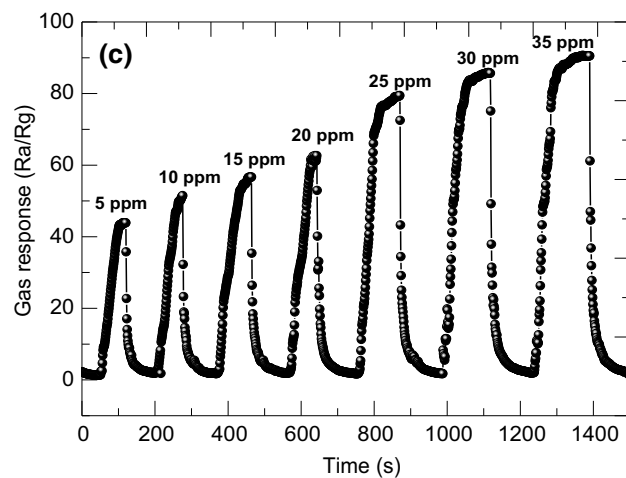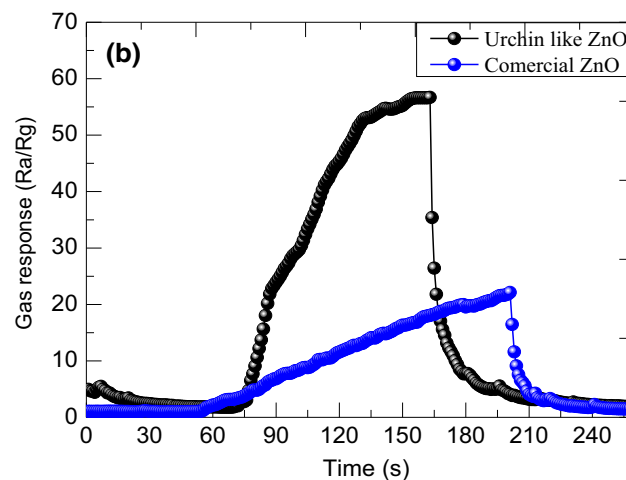When the ZnO nanostructure is exposed in the ambient air, oxygen molecules adsorb on the surface and capture

Fig. 8 a Gas responses of the sensors based on the urchin-like and commercial ZnO versus operating temperatures to 10 ppm acetone, **b** response-recovery time of the sensors based on the urchin-like and commercial ZnO to 10 ppm acetone at 300 °C, **c** real-time response and recovery curves of the sensor based on urchin-like ZnO to 5–35 ppm acetone at 300 °C and **d** gas responses of the sensor based on urchin-like ZnO to 10 ppm various target gases at 300 °C
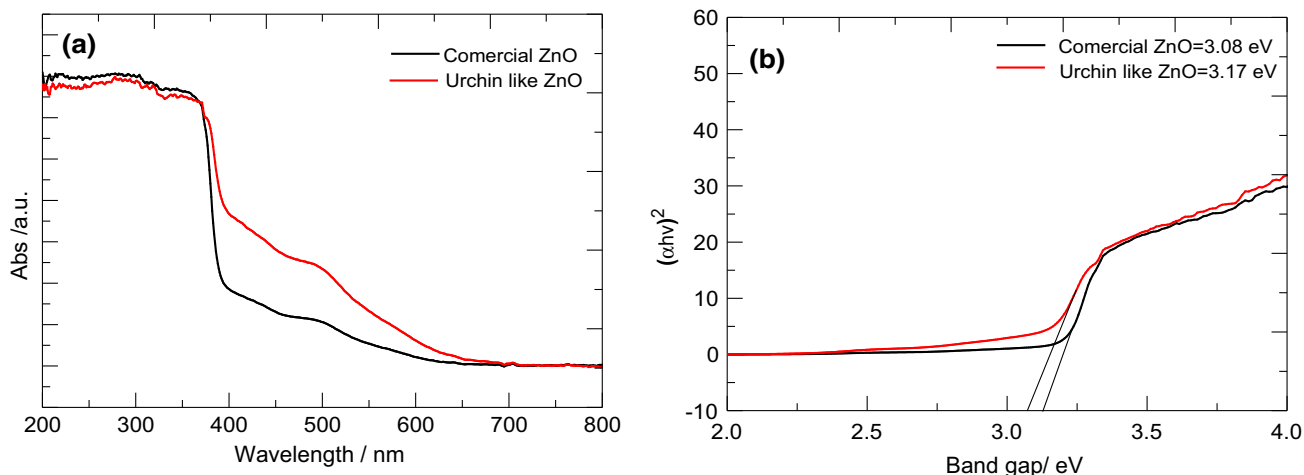
Fig. 9 **a** The UV–Vis absorbance and reflectance spectrum for urchin-like and commercial ZnO and **b** the $(\alpha h\upsilon)^2$ versus $h\upsilon$ curves of the UV–Vis spectra of the urchin-like and commercial ZnO
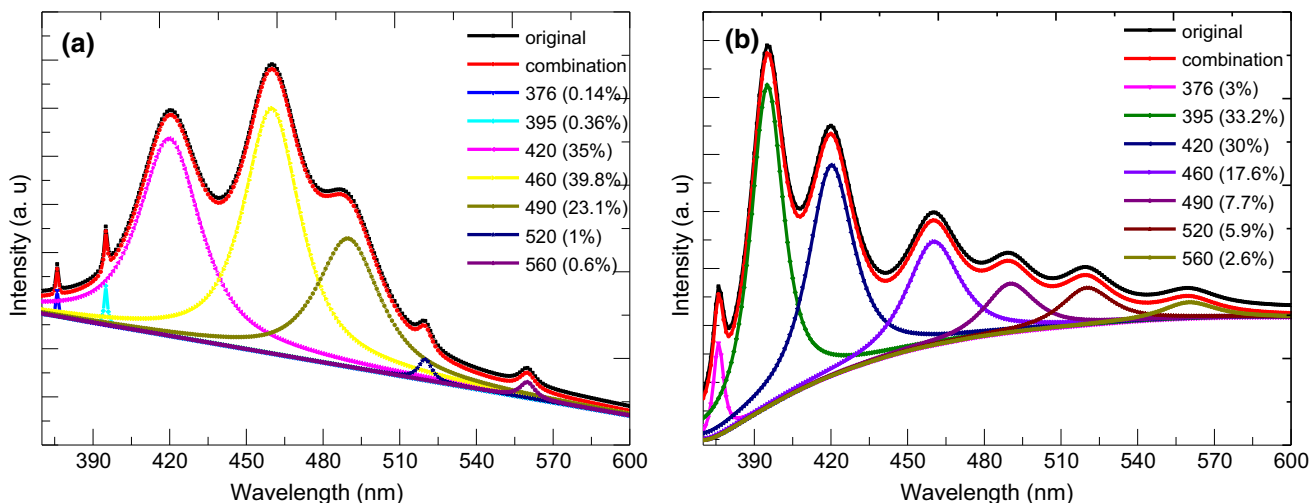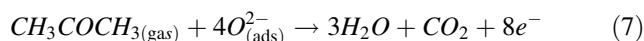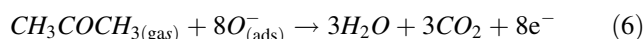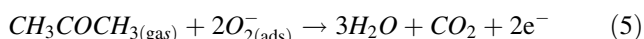

Fig. 10 The G–L decompositions of the PL spectra of **a** commercial ZnO and (**b**) urchin-like ZnO

free electrons from the conduction band of ZnO generating surface adsorbed oxygen ions, as represented by Eqs. (1)–(4).

$$O_{2(gas)} \rightarrow O_{2(ads)} \tag{1}$$

$$O_2 + e^- \rightarrow O^-_{2(ads)} \tag{2}$$

$$O_{2(ads)} + 2e^- \rightarrow 2O^-_{(ads)} \tag{3}$$

$$\frac{1}{2}O_{2(ads)} + 2e^- \rightarrow O^{2-}_{(ads)} \tag{4}$$

When the sample is exposed in HCHO, the HCHO molecules capture electrons from ZnO conduction band or react with absorbed oxygen ions,

$$CH_3COCH_{3(gas)} + 2O^-_{2(ads)} \rightarrow 3H_2O + CO_2 + 2e^- \tag{5}$$

$$CH_3COCH_{3(gas)} + 8O^-_{(ads)} \rightarrow 3H_2O + 3CO_2 + 8e^- \tag{6}$$

$$CH_3COCH_{3(gas)} + 4O^{2-}_{(ads)} \rightarrow 3H_2O + CO_2 + 8e^- \tag{7}$$

Equations (1)–(4) capture electrons from conduction band of ZnO, which results in the resistance increase. Equations (5)–(7) release electrons back to conduction band of ZnO, which results in the resistance decrease [30, 31].

The enhanced acetone gas sensing properties of the urchin-like hierarchical ZnO nanostructure can be attributed to the following aspects. Firstly, the narrowed band gap for urchin like ZnO making the electrons more easily to release from the conduction band to valance band and combined with O$_2$ forming more absorbed oxygen ions, which increased the gas sensing properties from one aspect.

Secondly, the enhanced acetone gas sensing properties can be understood from the important aspect of surface defects. It has been confirmed by the PL analyses that the urchin-like ZnO has the higher donors and fewer acceptors than that of commercial ZnO sample. More donors in ZnO is beneficial to the adsorption of oxygen and surface reaction. Thus, it can provide more electrons to the redox reaction of the absorbed acetone molecules, which contributes to the gas response. So the sensor based on urchin like ZnO exhibit better gas sensing performance than the sensor based on commercial ZnO. Thirdly, the unique structure of the as-prepared ZnO may be another possible reason for its superior gas sensing properties. On the one hand, the as-prepared 3D urchin-like ZnO nanostructure exhibits unique hierarchical structure. This hierarchical nanostructure can provide a large number of diffusion channels for the acetone gas, allow the internal surface of the material to be accessible to the acetone gas, thus generating two electron depleted layers on both surfaces of the individual ZnO nanosheet and offering more active sites necessary for the acetone gas oxidation, which result in an enhanced acetone gas sensing properties.

4 Conclusions

In summary, urchin-like ZnO nanostructures have been successfully synthesized based on a facile, environment-friendly (without any surfactant or organic solvent), simple one-step hydrothermal method. The urchin like ZnO was assembled by many nanorods and exhibited a unique hierarchical structure. The hydrothermal time and pH value have important effect on the morphology. UV–Vis spectra show that a narrower band gap for the urchin-like ZnO as compared to commercial ZnO. PL spectra indicate that the urchin like ZnO has the higher donors and fewer acceptors than that of commercial ZnO sample. The gas sensing measurement indicates that the urchin-like ZnO exhibited excellent gas sensing properties towards acetone as compared to commercial ZnO. The enhanced acetone gas sensing properties of the present ZnO nanostructure can be attributed to the narrowed band gap, surface defects and the unique hierarchical structure. The facile synthesis of the present ZnO nanostructure together with its superior gas sensing performance provides a potentially new approach for the design and construction of ZnO-based sensor.

References

1. M.M. Ayad, G.E. Hefnawey, N.L. Torad, A sensor of alcohol vapours based on thin polyaniline base film and quartz crystal microbalance. J. Hazard. Mater. **168**, 85–88 (2009)
2. S.J. Choi, I. Lee, B.H. Jang, D.Y. Youn, W.H. Ryu, C.O. Park, I.D. Kim, Selective diagnosis of diabetes using Pt-functionalized WO$_3$ hemitube networks as a sensing layer of acetone in exhaled breath. Anal. Chem. **85**, 1792–1796 (2013)
3. P. Sun, Y.X. Cai, S.S. Du, X.M. Xu, L. You, J. Ma, F.M. Liu, X.S. Liang, Y.F. Sun, G.Y. Lu, Hierarchical α-Fe$_2$O$_3$/SnO$_2$ semiconductor composites: hydrothermal synthesis and gas sensing properties. Sens. Actuators B Chem. **182**, 336–343 (2013)
4. M. Righettoni, A. Tricoli, S.E. Pratsinis, Si:WO$_3$ sensors for highly selective detection of acetone for easy diagnosis of diabetes by breath analysis. Anal. Chem. **82**, 3581–3587 (2010)
5. T.I. Nasution, I. Nainggolan, S.D. Hutagalung, K.R. Ahmad, Z.A. Ahmad, The sensing mechanism and detection of low concentration acetone using chitosan-based sensors. Sens. Actuators B Chem. **177**, 522–528 (2013)
6. T. Xiao, X.Y. Wang, Z.H. Zhao, L. Li, L. Zhang, H.C. Yao, J.S. Wang, Z.J. Li, Highly sensitive and selective acetone sensor based on C-doped WO$_3$ for potential diagnosis of diabetes mellitus. Sens. Actuators B Chem. **199**, 210–219 (2014)
7. P. Rai, Y.S. Kim, H.M. Song, Y.T. Yu, The role of gold catalyst on the sensing behavior of ZnO nanorods for CO and NO$_2$ gases. Sens. Actuators B Chem. **165**, 133–142 (2012)
8. P. Rai, Y.T. Yu, Synthesis of floral assembly with single crystalline ZnO nanorods and its CO sensing property. Sens. Actuators B Chem. **161**, 748–754 (2012)
9. P. Rai, Y.T. Yu, Citrate-assisted hydrothermal synthesis of single crystalline ZnO nanoparticles for gas sensor application. Sens. Actuators B Chem. **173**, 58–65 (2012)
10. P. Rai, S. Raj, K. Ko, K. Park, Y. Yu, Synthesis of flower-like ZnO microstructures for gas sensor applications. Sens. Actuators B Chem. **178**, 107–112 (2013)
11. S. Bai, L. Chen, D. Li, W. Yang, P. Yang, Z. Liu, A. Chen, C.L. Chung, Different morphologies of ZnO nanorods and their sensing property. Sens. Actuators B Chem. **146**, 129–137 (2010)
12. J. Elias, J. Michler, L. Philippe, M. Lin, C. Couteau, G. Lerondel, ZnO nanowires, nanotubes, and complex hierarchical structures obtained by electrochemical deposition. J. Mater. Sci. Electron. **40**, 728–732 (2011)
13. L. Yang, Y. Zhou, J. Lu, C. Li, Y. Liu, Y. Wu, M. Li, Controllable preparation of 2D and 3D ZnO micro-nanostructures and their photoelectric conversion efficiency. J. Mater. Sci. Electron. **27**, 1693–1699 (2016)
14. Y. Sun, Z. Wei, W. Zhang, P. Li, K. Lian, J. Hu, Synthesis of brush-like ZnO nanowires and their enhanced gas-sensing properties. J. Mater. Sci. Electron. **51**, 1428–1436 (2015)
15. M.R. Alenezi, S.J. Henley, N.G. Emerson, S.R.P. Silva, From 1D and 2D ZnO nanostructures to 3D hierarchical structures with enhanced gas sensing properties. Nanoscale **6**, 235–247 (2014)
16. I. Herman, J. Yeo, S. Hong, D. Lee, K.H. Nam, J.H. Choi, W.H. Hong, D. Lee, C.P. Grigoropoulos, S.H. Ko, Hierarchical weeping willow nano-tree growth and effect of branching on dye-sensitized solar cell efficiency. Nanotechnology **23**, 194005 (2012)
17. S.H. Ko, D. Lee, H.W. Kang, K.H. Nam, J.Y. Yeo, S.J. Hong, C.P. Grigoropoulos, H.J. Sung, Nanoforest of hydrothermally grown hierarchical ZnO nanowires for a high efficiency dye-sensitized solar cell. Nano Lett. **11**, 666–671 (2011)
18. W.W. Guo, Hollow and porous ZnSnO3 gas sensor for ethanol gas detection. J. Electrochem. Soc. **163**(5), B131–B139 (2016)

19. J.H. Lee, Gas sensors using hierarchical and hollow oxide nanostructures: overview. Sens. Actuators B Chem. **140**, 319–336 (2009)

20. J. Liu, Z.Y. Hub, Y. Peng, H.W. Huang, Y. Lia, M. Wu, X.X. Ke, G. van Tendeloo, B.L. Su, 2D ZnO mesoporous single-crystal nanosheets with exposed 0001 polar facets for the depollution of cationic dye molecules by highly selective adsorption and photocatalytic decomposition. Appl. Catal. B **181**, 138–145 (2016)

21. Y.J. Sun, Z.W. Zhao, F. Dong, W. Zhang, Mechanism of visible light photocatalytic NO_x oxidation with plasmonic Bi cocatalyst-enhanced $(BiO)_2CO_3$ hierarchical microspheres. Phys. Chem. Chem. Phys. **17**, 10383–10390 (2015)

22. L.X. Zhang, J.H. Zhao, H.Q. Lu, L.M. Gong, L. Li, J.F. Zheng, H. Li, Z.P. Zhu, High sensitive and selective formaldehyde sensors based on nanoparticle-assembled ZnO micro-octahedrons synthesized by homogeneous precipitation method. Sens. Actuators B Chem. **160**, 364–370 (2011)

23. H.C. Qin, W.Y. Li, Y.J. Xia, T. He, photocatalytic activity of heterostructures based on ZnO and N-doped ZnO. ACS Appl. Mater. Interfaces **3**, 3152–3156 (2011)

24. Y.H. Shi, M.Q. Wang, C. Hong, Z. Yang, J.P. Deng, X.H. Song, L.L. Wang, J.Y. Shao, H.Z. Liu, Y.C. Ding, Multi-junction joints network self-assembled with converging ZnO Nanowires as multi-barrier gas sensor. Sens. Actuators B Chem. **177**, 1027–1034 (2013)

25. N. Han, X.F. Wu, L.Y. Chai, H.D. Liu, Y.F. Chen, Counterintuitive sensing mechanism of ZnO nanoparticle based gas sensors. Sens. Actuators B Chem. **150**, 230–238 (2010)

26. S.L. Bai, T. Guo, Y.B. Zhao, J.H. Sun, D.Q. Li, A.F. Chen, C.C. Liu, Sensing performance and mechanism of Fe-doped ZnO microflowers. Sens. Actuators B Chem. **195**, 657–666 (2014)

27. M. Chen, Z.H. Wang, D.M. Han, F.B. Gu, G.S. Guo, Porous ZnO polygonal nanoflakes: synthesis, use in high-sensitivity NO_2 gas sensor, and proposed mechanism of gas sensing. J. Phys. Chem. C **115**, 12763–12773 (2011)

28. K. Ananda, O. Singh, M.P. Singh, J. Kaur, R.C. Singh, Hydrogen sensor based on graphene/ZnO nanocomposite. Sens. Actuators B Chem. **195**, 409–415 (2014)

29. W.W. Guo, T.M. Liu, J.X. Wang, W.J. Yu, R. Sun, Y. Chen, S. Hussai, X.H. Peng, Z.C. Wang, Hierarchical ZnO porous microspheres and their gas-sensing properties. Ceram. Int. **39**, 5919–5924 (2013)

30. S.Z. Deng, V. Tjoa, H.M. Fan, H.R. Tan, D. Sayle, M. Olivo, S. Mhaisalkar, J. Wei, C.H. Sow, Reduced grapheme oxide conjugated Cu_2O nanowire meso-crystals for high-performance NO_2 gas sensor. J. Am. Chem. Soc. **134**, 4905–4917 (2012)

31. F. Vietmeyer, B. Seger, P.V. Kamat, Anchoring ZnO particles on functionalized single wall carbon nanotubes. Excited state interactions and charge collection. Adv. Mater. **19**, 2935–2940 (2007)